



# CHALMERS

## Chalmers Publication Library

### **The influence of contact modelling on simulated wheel/rail interaction due to wheel flats**

This document has been downloaded from Chalmers Publication Library (CPL). It is the author's version of a work that was accepted for publication in:

**Wear (ISSN: 0043-1648)**

Citation for the published paper:

Pieringer, A. ; Kropp, W. ; Nielsen, J. (2014) "The influence of contact modelling on simulated wheel/rail interaction due to wheel flats". *Wear*, vol. 314(1-2), pp. 273-281.

<http://dx.doi.org/10.1016/j.wear.2013.12.005>

Downloaded from: <http://publications.lib.chalmers.se/publication/197497>

Notice: Changes introduced as a result of publishing processes such as copy-editing and formatting may not be reflected in this document. For a definitive version of this work, please refer to the published source. Please note that access to the published version might require a subscription.

Chalmers Publication Library (CPL) offers the possibility of retrieving research publications produced at Chalmers University of Technology. It covers all types of publications: articles, dissertations, licentiate theses, masters theses, conference papers, reports etc. Since 2006 it is the official tool for Chalmers official publication statistics. To ensure that Chalmers research results are disseminated as widely as possible, an Open Access Policy has been adopted. The CPL service is administrated and maintained by Chalmers Library.

(article starts on next page)

# The influence of contact modelling on simulated wheel/rail interaction due to wheel flats

A. Pieringer<sup>a,\*</sup>, W. Kropp<sup>a</sup>, J.C.O Nielsen<sup>b</sup>

<sup>a</sup>*Division of Applied Acoustics / CHARMEC, Chalmers University of Technology, 412 96 Gothenburg, Sweden*  
<sup>b</sup>*Department of Applied Mechanics / CHARMEC, Chalmers University of Technology, 412 96 Gothenburg, Sweden*

---

## Abstract

Most available wheel/rail interaction models for the prediction of impact forces caused by wheel flats use a Hertzian spring as contact model and do not account for the changes in contact stiffness due to the real three-dimensional wheel flat geometry. In the literature, only little information is available on how this common simplification influences the calculation results. The aim of this paper is to study the influence of contact modelling on simulated impact forces due to wheel flats in order to determine the errors introduced by simplified approaches. For this purpose, the dynamic wheel/rail interaction is investigated with a time-domain model including a three-dimensional (3D) non-Hertzian contact model based on Kalker's variational method. The simulation results are compared with results obtained using a two-dimensional (2D) non-Hertzian contact model consisting of a Winkler bedding of independent springs or alternatively a single non-linear Hertzian contact spring. The relative displacement input to the Hertzian model is either the wheel profile deviation due to the wheel flat or the pre-calculated vertical wheel centre trajectory. Both the 2D model and the Hertzian spring with the wheel centre trajectory as input give rather similar results to the 3D model, the former having the tendency to slightly underestimate the maximum impact force and the latter to slightly overestimate. The Hertzian model with the wheel profile deviation as input can however lead to large errors in the result. Leaving aside this contact model, the correct modelling of the longitudinal geometry of the wheel flat, is actually seen to have a larger influence on the maximum impact force than the choice of contact model.

*Keywords:* wheel flat, wheel/rail interaction, non-Hertzian contact, Hertzian contact, time-domain modelling

---

## 1. Introduction

A wheel flat is a defect of the running surface of a railway wheel, giving rise to noise and safety problems. This type of wheel damage occurs when the wheel locks and slides along the rail because of malfunctioning brakes or because the braking force is too high in relation to the available wheel/rail friction. Leaves, grease, frost and snow on the rail surface may aggravate the problem. As a consequence, a part of the wheel tread is worn off and locally the wheel temperature is raised significantly. When the wheel starts rolling again, this is followed by a rapid cooling due to the conduction into the large steel volume surrounding the flat. This process may lead to material phase transformations (formation of martensite) and residual stresses beneath the wheel flat [1].

A wheel with a flat generates large impact forces. As a consequence, large vibration amplitudes of wheel and rail occur, resulting in high noise radiation. Furthermore, these impact forces may cause significant damage to the track, causing for example the initiation and propagation of fatigue cracks. Further damage to the wheel is also likely to occur. Cracking in the brittle martensite leads eventually to large pieces of metal breaking off from the wheel tread, a phenomenon known as spalling [1].

The prediction of the dynamic interaction of railway wheel and track in response to discrete irregularities of the running surface such as wheel flats requires the application of time-domain models. In contrast to frequency-domain models, time-domain models are able to include a non-linear contact model. Non-linearities in the wheel/rail contact cannot be neglected in the case of excitation by wheel flats because of the resulting large contact forces and the occurrence of loss of contact for train speeds above the critical speed [2, 3].

Most available interaction models for the prediction of impact forces caused by wheel flats use a Hertzian spring as contact model and introduce the wheel flat as relative displacement excitation between wheel and rail, e.g. the models [4–9]. Wu and Thompson [8] improved the Hertzian contact model for wheel flats by accounting for the finite size of the wheel. They introduced a relative displacement excitation based on the vertical wheel centre trajectory which differs from the geometric shape of the wheel flat. This approach is similar to considering the contact filter effect [10] for wheel/rail interaction due to roughness excitation.

Nevertheless, all models using a Hertzian contact spring have in common that they rely on one effective contact point and a simplified geometry of the wheel flat. Further, they do not account for the changes in contact stiffness due to the real three-dimensional (3D) wheel flat geometry. In the literature, only little information is available on how these common simplifications influence the calculation results. Baeza et al. [11] com-

---

\*Corresponding author. Tel.: +46 31 772 2209; fax: +46 31 772 2212.  
Email address: astrid.pieringer@chalmers.se (A. Pieringer)

pared the dynamic response due to wheel flats obtained from the Hertzian model (accounting for the finite size of the wheel according to [8]) and a 3D non-Hertzian model. It was concluded that the Hertzian model tends to overestimate the peak impact force. Zhu et al. [12] concluded that the impact forces obtained with a two-dimensional (2D) continuous bedding model differ considerably from results obtained with the Hertzian model (not accounting for the finite size of the wheel according to [8]). An earlier study by Pieringer et al. [10] on wheel/rail dynamic interaction due to roughness excitation showed that the choice of contact model and the detailedness of the considered roughness data significantly influence the simulation results.

The aim of this paper is to study in detail the influence of contact modelling on simulated impact forces due to wheel flats. For this purpose, the dynamic wheel/rail interaction caused by a wheel flat is investigated with the time-domain interaction model from [10] which accounts for the 3D geometry of the wheel flat. The implemented contact model is based on an influence-function method for the elastic halfspace and considers the 3D running surfaces of the rail and the wheel featuring the flat. To allow for an investigation of the influence of the contact modelling on the calculation results, the interaction model is also used with two simpler contact models. The first such contact model is a 2D model consisting of a Winkler bedding of independent springs. This model uses a simplified wheel and rail geometry and a 2D description of the wheel flat. The second simplified contact model is a Hertzian contact spring.

In a first step, the wheel/rail interaction model together with the 3D contact model is applied to study the dynamic response due to different types of wheel flats. Parameters investigated include the shape and dimensions of the wheel flat, the train speed and the impact position on the rail in relation to the discrete supports.

In a second step, selected simulations are repeated with the 2D and Hertzian contact models, in order to assess the errors introduced by these simpler contact models in comparison to the 3D model. The study will thus address the question of which level of contact model complexity is needed to calculate the dynamic wheel/rail interaction due to wheel flats.

## 2. Description of wheel flats

In published prediction models, the shape of the wheel flats is almost exclusively described by simple analytic functions. Measured wheel profiles have been used in [7]. In the absence of measurement data, the current study also uses analytical functions. Two types of wheel flat geometries are considered: the newly formed wheel flat with sharp edges as occurring right after formation and the rounded wheel flat, which rapidly develops from the newly formed flat as a result of wheel tread wear and plastic deformation, see Fig. 1. Further wheel damage as spalling is not taken into account.

The two-dimensional shape of the idealised newly formed wheel flat can be modelled as a chord of the wheel circumference. The length  $l_0$  of the newly formed wheel flat is related to

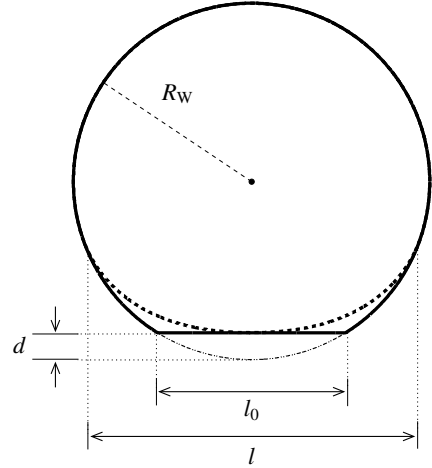


Figure 1: Idealized 2D geometry of newly formed and rounded wheel flats (size of the wheel flats exaggerated).

its depth  $d$  according to

$$l_0 \approx \sqrt{8R_W d}, \quad (1)$$

where  $R_W$  is the wheel radius and it has been assumed that the depth of the flat is small in comparison to the wheel radius. The vertical wheel profile deviation (i.e. the difference between the surface of the undamaged wheel and the wheel featuring the flat) for a newly formed flat is approximately given by

$$z_{\text{nf}} \approx d - \frac{x^2}{2R_W}, \quad -\frac{l_0}{2} \leq x \leq \frac{l_0}{2}, \quad (2)$$

where  $x$  describes the horizontal distance from the centre of the wheel flat.

The rounded flat is assumed to have the same depth  $d$  as the newly formed flat, but a length  $l > l_0$ . Following the approach in [4], the vertical profile deviation of the rounded wheel flat is described by

$$z_{\text{rf}}(x) = \frac{d}{2} \left( 1 + \cos\left(2\pi \frac{x}{l}\right) \right), \quad -\frac{l}{2} \leq x \leq \frac{l}{2}. \quad (3)$$

In order to guarantee that  $z_{\text{rf}}(x) \geq z_{\text{nf}}(x)$  for all  $x$  (i.e. the rounded wheel flat is at least as deep as the new wheel flat), the length of the rounded flat has to satisfy  $l \geq \pi/2 l_0$ .

It is not evident how to model the three-dimensional shape of wheel flats, which is required as input to the 3D contact model. In the current study, the approach by Baeza et al. [11] has been adopted, where it is assumed that the shape of the newly formed flat corresponds to the shape of the rail head on which it was formed. Cylindrical profiles have been used for both wheel and rail and Fig. 2(a) shows an example of the flat shape obtained by this means. For the newly formed flat, parameter lines of the vertical wheel profile deviation in the rolling direction are of the type given in Eq. (2), while parameter lines in the transverse direction are circular arcs with rail head radius  $R_R$ . Analogously, parameter lines of the vertical wheel profile deviation for the rounded flat in the rolling direction are assumed of the type given in Eq. (3), while parameter lines in the transverse direction are circular arcs with rail head radius  $R_R$  (Fig. 2(b)). In

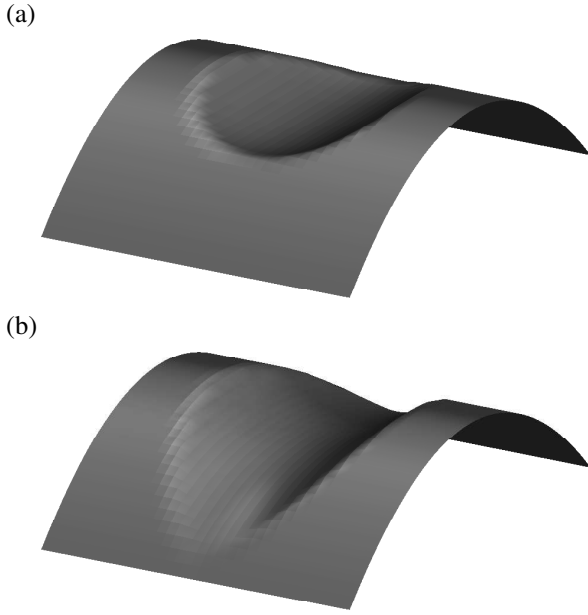


Figure 2: Idealized 3D geometry of (a) a newly formed and (b) a rounded wheel flat on a section of the cylindrical wheel surface (size of the wheel flats and width of the wheel exaggerated).

practice, the shape of wheel flats will differ from the idealized shapes considered in this study.

### 3. Wheel/rail interaction model

The wheel/rail interaction model, which is illustrated in Fig. 3, is described in detail in [13] and has been earlier presented in [10]. In order to facilitate the task for the reader, the description from [10] is partly repeated here. Adaptations have been made to excitation by wheel flats where necessary, see Section 3.3.

The wheel/rail interaction model is formulated in the time-domain and includes a linear wheel model and a linear track model, which are coupled through a non-linear contact model describing the local elastic deformation of wheel and rail. Only vertical wheel/rail interaction is considered. For inclusion into the interaction model, the wheel and track are represented by pre-calculated impulse response functions (also denoted Green's functions) [13]. This representation leads to an interaction model that is computationally very efficient.

#### 3.1. Wheel model

The wheel model is a two degree-of-freedom model [8, 14] containing half the wheelset mass  $M_W$  and the primary suspension stiffness  $k_S$  and damping  $c_S$ , see Fig. 3. The vehicle system above the primary suspension of the wheelset is simplified to a static preload,  $P$ . The small mass  $m_W$ , the extra spring with constant  $k_W$  and the extra viscous damper with constant  $c_W$  can be used to tune the receptance of this simplified model to roughly resemble the receptance obtained with a more detailed finite-element model of the wheelset, see [14]. Most resonances and

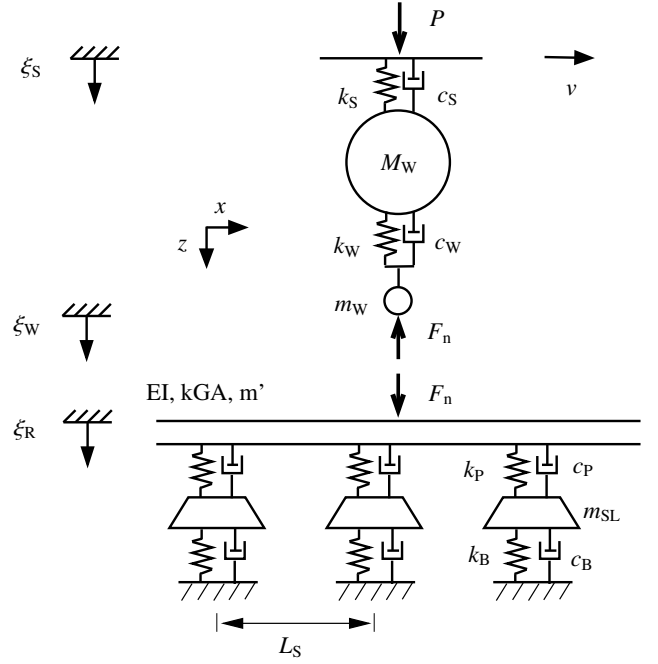


Figure 3: Principle sketch of the dynamic wheel/rail interaction model.

antiresonances of the wheelset cannot be captured by the simplified model, but the average of the receptance at frequencies above about 1000 Hz is similar for both models. The numerical parameters used are presented in Table 1. In the interaction model, the wheel moving along the rail with train speed  $v$  is represented by its Green's function  $\tilde{g}_W(t)$ . The vertical displacement  $\xi_W(t)$  of the wheel is calculated by convoluting the normal contact force  $F_n(t)$  with the Green's function of the wheel

$$\xi_W(t) = - \int_0^t F_n(\tau) \tilde{g}_W(t - \tau) d\tau + \xi_S(P), \quad (4)$$

where  $\xi_S(P)$  is the position of the primary suspension corresponding to the static preload  $P$ .

Table 1: Parameters of the wheel model.

Half the wheelset mass (kg)	$M_W$	593
Stiffness of primary suspension (N/m)	$k_S$	$1.12 \cdot 10^6$
Damping of primary suspension (Ns/m)	$c_S$	$13.2 \cdot 10^3$
Small mass (kg)	$m_W$	3.0
Extra stiffness (N/m)	$k_W$	$2.4 \cdot 10^9$
Extra damping (Ns/m)	$c_W$	$155 \cdot 10^3$
Wheel radius (m)	$R_W$	0.45
Static preload (N)	$P$	$118 \cdot 10^3$

#### 3.2. Track model

The track model used in this study is the linear finite element model accounting for discrete supports, which has been presented by Nielsen and Igeland in [6]. The model comprises a 60E1 rail represented by undamped Rayleigh-Timoshenko beam elements. The discrete supports consist of railpads and

sleepers on ballast, see Fig. 3. The track model is 70 sleeper bays long and has clamped boundaries at the two rail ends. The numerical parameters used are presented in Table 2. In the wheel/rail interaction model, the discretely supported rail is represented by moving Green's functions,  $\tilde{g}_{R,v}^{x_0}(t)$  [13, 15]. For excitation of the rail (index R) at the position  $x_0$  at time  $t_0 = 0$ , the function  $\tilde{g}_{R,v}^{x_0}(t)$  describes the displacement response of the rail at a point moving at train speed  $v$  away from the excitation, thus at the nominal contact point between wheel and rail. The train speed  $v$  is assumed constant.

Table 2: Parameters of the track model.

Bending stiffness of rail (Nm <sup>2</sup> )	$EI$	$6.4 \cdot 10^6$
Shear stiffness of rail (N)	$kGA$	$250 \cdot 10^6$
Rail mass per unit length (kg/m)	$m'$	60
Rail head radius (m)	$R_R$	0.30 (0.45)
Sleeper spacing (m)	$L_S$	0.65
Railpad stiffness (N/m)	$k_p$	$120 \cdot 10^6$
Railpad damping (Ns/m)	$c_p$	$16 \cdot 10^3$
Sleeper mass (half) (kg)	$m_{SL}$	125
Ballast stiffness per half sleeper (N/m)	$k_B$	$140 \cdot 10^6$
Ballast damping per half sleeper (Ns/m)	$c_B$	$165 \cdot 10^3$

The vertical displacement  $\xi_R(t)$  of the rail at the contact point is obtained by convoluting the contact force  $F_n(t)$  with the moving Green's functions

$$\xi_R(t) = \int_0^t F_n(\tau) \tilde{g}_{R,v}^{x_0}(t - \tau) d\tau. \quad (5)$$

### 3.3. Contact models

The wheel/rail interaction model can be used with different contact models. Three alternative contact models are considered in this paper.

#### 3.3.1. 3D contact model

The most detailed of the three contact models used is an implementation of Kalker's variational method [16]. This model considers the three-dimensional running surfaces of the rail and the wheel including the three-dimensional shape of the wheel flat. The materials of wheel and rail are assumed linearly elastic and wheel and rail are locally approximated by elastic half-spaces. Dividing the potential contact area into  $N_e$  rectangular elements, the following relation holds

$$\mathbf{u} = \mathbf{C} \mathbf{p}, \quad (6)$$

where the vectors  $\mathbf{u}$  and  $\mathbf{p}$  contain, respectively, the combined normal surface displacement of wheel and rail and the contact pressure in all elements. The influence coefficients contained in the matrix  $\mathbf{C}$  can be found e.g. in [16]. The total contact force  $F_n$  is obtained by summing the contributions from the different elements

$$F_n = \sum_{e=1}^{N_e} p_e A_e, \quad (7)$$

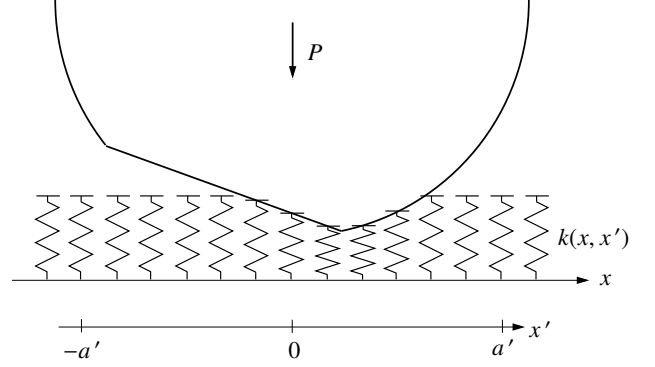


Figure 4: Bedding model of the wheel/rail contact.

where  $A_e$  is the area of element  $e$ . Introducing the vector  $\mathbf{d}$  of distance between the deformed bodies, with elements  $d_e$ , the contact conditions are formulated as

$$\begin{aligned} d_e &\geq 0, \\ p_e &\geq 0, \\ d_e p_e &= 0. \end{aligned} \quad (8)$$

If contact occurs in a surface element, the distance is zero and the contact pressure is positive. If contact does not occur, the distance is positive and the pressure is zero. Adhesion (i.e. negative pressure) and penetration (i.e. negative distance) are excluded by (8). The elements of the vector  $\mathbf{d}$  are obtained as

$$d_e = \xi_R - \xi_W - r_e + z_{Re} - z_{We} + u_e, \quad (9)$$

where the vector  $\mathbf{r}$  contains the wheel profile deviation due to the wheel flat. Additionally, the vector  $\mathbf{r}$  may contain the combined wheel and rail roughness ( $\mathbf{r}_W - \mathbf{r}_R$ ) in the contact area. The vectors  $\mathbf{z}_R$  and  $\mathbf{z}_W$  contain the profiles of the undamaged and smooth wheel and rail.

Eqs. (4)-(9) together with the relation

$$x = vt \quad (10)$$

form a non-linear system of equations that can be solved for each wheel centre position  $x$  on the rail, e.g. by combining the Newton-Raphson method with an active set strategy [13, 16].

#### 3.3.2. 2D contact model

The second contact model originating from an approach by Ford and Thompson [17] is a two-dimensional model consisting of a Winkler bedding of independent springs introduced between wheel and rail, see Fig. 4. This model takes into account the two-dimensional wheel profile deviation due to the wheel flat in the rolling direction.

Ideally, the bedding should correctly model the contact length, the total contact load and the deflection as predicted by Hertzian theory if wheel and rail are smooth and undamaged. Additionally, the wheel geometry (radius) should be modelled correctly. However, as the springs of the bedding are uncoupled, only three of these four quantities can be represented correctly at the same time. In the case of roughness excitation in

the context of rolling noise, it is important to capture the right contact length which affects the roughness wavelengths filtered in the contact patch. The best compromise is then to adjust the wheel radius [17]. In the case of excitation by wheel flats, the geometry of the wheel and the wheel flat is yet of primary importance. Especially, the (minimum) circumferential curvature of the wheel tread has been found to have a big influence on the impact force [18]. In the current study, it has therefore been decided to use the correct wheel radius, and total contact load and deflection, which leads to an incorrect contact length. For simplicity, it has been additionally assumed that the transverse radius of curvature  $R_R$  of the rail (which is straight in the rolling direction) is equal to the rolling radius  $R_W$  of the cylindrical wheel [17].

For the wheel centre positioned at  $x$ , the deflection  $\Delta\zeta(x, x')$  of all involved contact springs depends on the wheel displacement  $\xi_W(x)$ , the rail displacement  $\xi_R(x)$ , the wheel profile deviation due to the wheel flat  $r(x, x')$ , and the circular wheel profile in the rolling direction  $z_W(x')$ , as

$$\Delta\zeta(x, x') = \xi_W(x) - \xi_R(x) + r(x, x') + z_W(x'). \quad (11)$$

The total contact force is obtained by integration over the bedding

$$F_n(x) = \int_{-a'}^{a'} \tilde{k}(x, x') \Delta\zeta(x, x') dx', \quad (12)$$

which has a stiffness per unit length

$$\tilde{k}(x, x') = \begin{cases} \frac{1}{2\sqrt{2}} \frac{E}{1-\nu^2} & \text{for } \Delta\zeta(x, x') \geq 0 \\ 0 & \text{for } \Delta\zeta(x, x') < 0 \end{cases}, \quad (13)$$

where  $E$  is the Young's modulus and  $\nu$  the Poisson's ratio of rail and wheel (assumed to be of the same material). The integration domain,  $[-a', a']$ , has to be chosen long enough to include all potential points of contact. Note that the stiffness  $\tilde{k}$  in Eq. (13) differs from the stiffness used in the original version of the 2D model [17], which has been applied in [10] for roughness excitation.

Eqs. (4), (5) and (10)-(13) form a non-linear system of equations that can be solved for each wheel centre position  $x$  on the rail.

### 3.3.3. Hertzian contact model

A single non-linear Hertzian spring is introduced as the third contact model. The force-deflection relation can be written as

$$F_n(x) = \begin{cases} C_H (\Delta\zeta(x))^{3/2} & \text{for } \Delta\zeta(x) \geq 0 \\ 0 & \text{for } \Delta\zeta(x) < 0 \end{cases}, \quad (14)$$

where

$$C_H = \frac{2}{3} \frac{E}{1-\nu^2} \sqrt{R} \quad (15)$$

is the Hertzian constant and wheel and railhead radius of curvature  $R$  are taken as equal. The kinematic constraint equation reads

$$\Delta\zeta(x) = \xi_W(x) - \xi_R(x) + r_{eq}(x), \quad (16)$$

where  $r_{eq}$  is the relative displacement input describing the excitation of the wheel/rail system by the wheel flat. Two different methods to obtain  $r_{eq}$  are considered:

- The relative displacement input corresponds to the vertical wheel profile deviation given in Eqs. (2) and (3) for the newly formed and the rounded wheel flat, respectively.
- The pre-calculated vertical trajectory of the wheel centre when the wheel flat passes through the contact zone is used as relative displacement input. The trajectory is obtained for a rigid wheel rolling on a rigid rail without loss of contact according to the procedure described by Wu and Thompson in [8].

Fig. 5 shows examples of the relative displacement input obtained with the two methods.

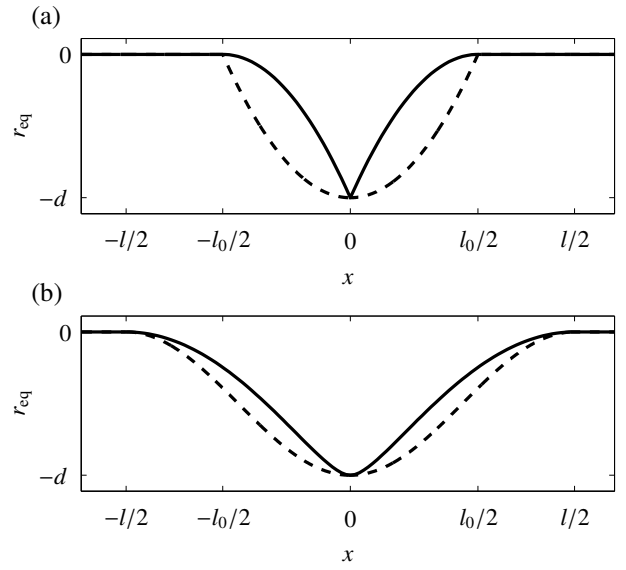


Figure 5: Examples of relative displacement input  $r_{eq}$  for the Hertzian model: --- wheel profile deviation; — vertical wheel centre trajectory; (a) newly formed wheel flat with depth  $d$  and length  $l_0$ ; (b) rounded wheel flat with depth  $d$  and length  $l = 1.76 l_0$ .

Eqs. (4), (5), (10) and (14)-(16) form a system of non-linear equations that can be solved for each wheel centre position  $x$  on the rail.

### 3.4. Advantages and limitations of the modelling approach

The chosen modelling approach based on Green's functions is computationally efficient since the Green's functions representing wheel and track can be pre-calculated before carrying out the time-stepping procedure. Consequently, the calculation time of dynamic simulations with the wheel/rail interaction model is mainly determined by the choice of contact model. On the one hand, the usage of Green's functions implies a simplification since only linear wheel and track models can be represented by Green's functions. On the other hand, this approach is very versatile because any wheel or track represented by Green's functions can be used without changing the mathematical formulation of the interaction model. The rigid wheel model and the Timoshenko beam model of the track used in this article are considered sufficient if only vertical wheel/rail interaction is of interest [19]. The inclusion of a flexible wheel

model and a track model accounting for the cross-sectional deformations of the rail – as needed for an extension to tangential interaction – is straightforward [20].

All three contact models used in this article are non-linear in terms of the force/deflection relationship, but wheel and rail materials are assumed to be linearly elastic. Furthermore, the contact models are all quasi-static, which implies that local inertial effects in the contact area are not modelled. It is not known whether these local effects are required for the modelling of impact forces due to wheel flats. However, one should keep in mind this simplification when interpreting the simulation results. The most detailed of the contact models used – the 3D model – is based on the half-space assumption, which is valid if the contact area is small in comparison to the radii of curvature of the wheel and rail surfaces. This criterion is generally fulfilled for the contact between an undamaged wheel tread and the top of the rail. The half-space assumption should still be valid in the presence of smaller wheel flats, but its validity is questionable in the case of larger wheel flats, where larger contact areas can occur. General material models, local dynamic effects and arbitrary wheel/rail geometry could be considered when the wheel/rail interaction is modelled by a transient dynamic finite element model, such as e.g. [21–23]). However, such models lead to considerably longer calculation times limiting the possibility of parameter studies and the applicability of the models for engineering tasks. To the knowledge of the authors, results for impact forces due to wheel flats calculated with transient dynamic finite element models are not available in the literature.

#### 4. Impact forces due to wheel flats

In this section, the wheel/rail interaction model as described in Section 3 is applied to calculate impact forces due to wheel flats. The simulations in Sections 4.1 and 4.2 are carried out with the 3D contact model, while simulations with all four contact models are compared in Section 4.3.

The 3D contact model can consider the actual transverse wheel and rail profiles. It is however desirable to use the same type of wheel and rail profiles in all contact models for the comparison. As the 2D contact model in the form used in this study requires that the transverse radius of the rail is set equal to the wheel rolling radius  $R_W = 0.45$  m, cylindrical profiles  $z_W$  and  $z_R$  both of radius  $R_W$  are used in the 3D contact model. The only exception is Section 4.1, where simulation results from the 3D model are compared to field measurements. Here, the original transverse radius of the rail  $R_R = 0.30$  m has been kept.

In the 2D contact model the element length is 1 mm, and in the 3D contact model square elements with a side length of 1 mm are used.

##### 4.1. Comparison of simulation results with field measurements

To demonstrate the accuracy of the modelling approach, results from simulations with the 3D contact model are compared with field measurements from reference [24] in terms of the maximum impact load, see Fig. 6.

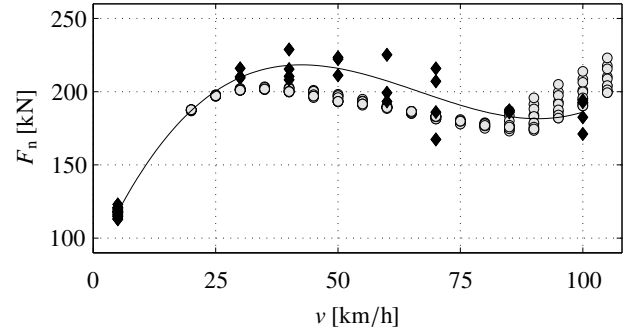


Figure 6: Measured maximum impact forces ( $\blacklozenge$ , black) due to a 0.9 mm deep rounded wheel flat from reference [24] in comparison to calculated maximum impact forces ( $\circ$ ) with the 3D contact model. Calculations with 10 different initial angular positions of the wheel at each train speed in order to cover the range of impact positions relative to the discrete supports. A third-degree polynomial fitted to the measurement data is also shown.

In the field test, the impact load caused by a rounded wheel flat with depth  $d = 0.9$  mm and length  $l = 0.1$  m on a freight wagon with axle load 24 metric tonnes (i.e. static preload  $P \approx 118$  kN) was measured for train speeds between 30 km/h and 100 km/h. The measurements were carried out using a wheel impact load detector that was based on strain gauges mounted on the rail web in nine consecutive sleeper bays. The impact load detector was calibrated against the quasi-static wheel load that was measured when the train passed the test site at a speed of 5 km/h [24]. As the receptance of the loaded track in the frequency range of interest could not be measured during the field test, Nielsen et al. determined the rail pad and ballast parameters through model calibration with the wheel/rail interaction model DIFF [25]. These model parameters (listed in Table 2) are also used in the present simulations. The 3D shape of the wheel flat was not measured during the field test.

The calculated impact force varies depending on where the wheel flat hits the rail in relation to the sleeper location. In order to cover the whole range of maximum impact force magnitudes, simulations with 10 different initial angular wheel positions are run. The location of the wheel section with the wheel flat in reference to the rail at the beginning of the simulation determines the running distance after which the wheel flat enters the contact zone and influences consequently where the impact occurs with regard to the sleepers.

Taking into account the uncertainty in the track parameters and in the geometry of the wheel flat, the level of agreement between simulations and measurements seen in Fig. 6 is encouraging.

##### 4.2. Parameter study with the 3D contact model

In this Section, the most complete of the contact models introduced in Section 3.3 – the 3D contact model – is applied to study the influence of different parameters on the dynamic response due to wheel flats.

Fig. 7 shows the calculated maximum and minimum contact forces for train speeds from 20 km/h to 300 km/h. In addition to the 0.9 mm deep rounded wheel flat with length 0.1 m from

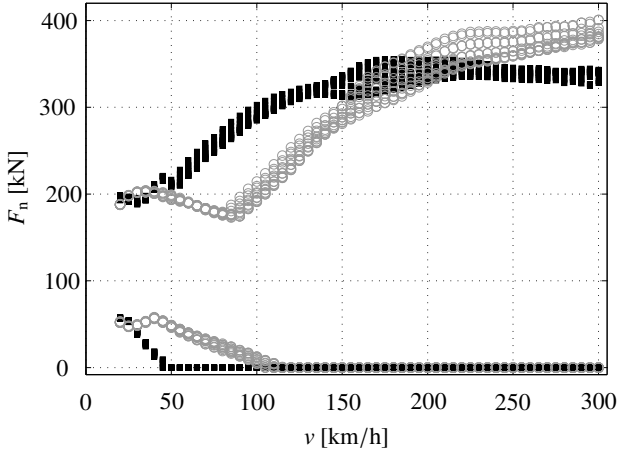


Figure 7: Maximum and minimum contact forces due to a rounded (O) and a new (■) 0.9 mm deep wheel flat. Calculations with the 3D contact model and with 10 different initial angular positions of the wheel at each train speed in order to cover the range of impact positions relative to the discrete supports.

Section 4.1, also a 0.9 mm deep new wheel flat is considered. In the case of the rounded wheel flat, the curve showing the maximum impact force has a local maximum at 35 km/h and a local minimum at 85 km/h. Above this train speed, to begin with the curve increases approximately linearly, but levels out at higher train speeds. Loss of contact occurs for the first time at 105 km/h. The new wheel flat causes higher maximum impact forces than the rounded wheel flat in the speed range from 40 km/h to 180 km/h (and at 20 km/h) and lower forces otherwise. For the new wheel flat, loss of contact occurs already at 45 km/h.

The calculations from Fig. 7 have been carried out with 10 different initial angular wheel positions at each train speed in order to cover the range of possible impact positions in relation to the discrete supports. For the same type of wheel flat, the highest maximum impact force is up to 14% higher than the lowest maximum impact force at the same train speed.

Fig. 8 illustrates the influence of the flat depth on the maximum impact force due to rounded wheel flats. The rounded wheel flats with depths ranging from 0.25 mm to 2.00 mm are assumed to have the length  $l = 1.76 l_0$ , with  $l_0$  being the length of the new wheel flat with the same depth. As seen in Fig. 8, the larger the flat depth, the higher the maximum impact force and the earlier occurs loss of contact. While loss of contact is already observed at 30 km/h for the flat with depth 2.00 mm, it does not occur below 240 km/h for the 0.25 mm flat.

The speed dependency of the curves is principally similar for the different depths, but the local maximum and minimum of the curves are more pronounced for higher depths and are also moved to higher train speeds. The smaller the flat depth (and thereby the flat length), the earlier the curve flattens out at higher train speeds.

### 4.3. Comparison of the different contact models

To assess the accuracy of the other contact models in comparison to the 3D contact model, the calculations for a rounded

wheel flat with depths 0.9 mm (Fig. 7) and 0.5 mm and 1.75 mm (Fig. 8) have been repeated with the 2D contact model and the two versions of the Hertzian model. The maximum of the maximum impact forces from 8 simulations with different initial angular positions of the wheel has been considered for the comparison between the contact models. The results are presented in Fig. 9 in terms of the maximum impact force magnitudes for all contact models and in Fig. 10 as the relative deviation from the results obtained with the 3D contact model. Besides the rounded wheel flats, results for the corresponding new wheel flats with the same flat depth are also shown in Figs. 9 and 10.

A first observation from Figs. 9 and 10 is that the Hertzian model with the wheel profile deviation as input leads to large deviations from the 3D contact model, while the other models give relatively similar results. The deviations are generally larger for the new wheel flats in comparison to the rounded wheel flats.

When the wheel profile deviation due to the wheel flat is used as relative displacement input in the Hertzian model, it is ignored that the wheel has a finite size and that its vertical motion therefore differs from the wheel profile deviation. This leads to large errors in the simulation results: in the examples in Figs. 9 and 10, up to 24% overestimation for the rounded wheel flats and up to 124% overestimation for the new wheel flats. Especially in the case of new wheel flats, the model does not seem suitable for quantitative prediction of impact forces due to wheel flats.

However, the Hertzian model with the pre-calculated vertical wheel centre trajectory as relative displacement input performs fairly well in comparison to the 3D model. The model has the tendency to overestimate the maximum impact force. Deviations from the 3D model in Figs. 9 and 10 reach up to 8% and 18% for the rounded and new wheel flats, respectively. In their comparison of contact models (for different model parameters),

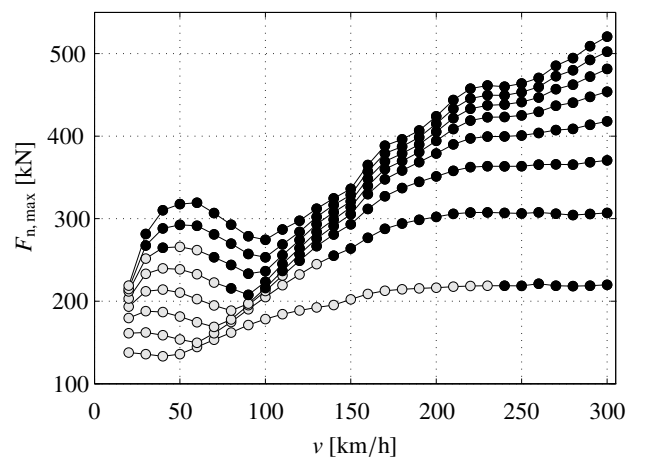


Figure 8: Maximum impact forces due to a rounded wheel flat as function of train speed and flat depth. The lines correspond (from lower to upper) to the depths [0.25, 0.50, 0.75, 1.00, 1.25, 1.50, 1.75, 2.00] mm. Calculations with the 3D contact model. The maximum of the maximum impact forces from 8 simulations with different initial angular positions of the wheel is shown. Black circles indicate that loss of contact occurs for at least one of these 8 simulations.

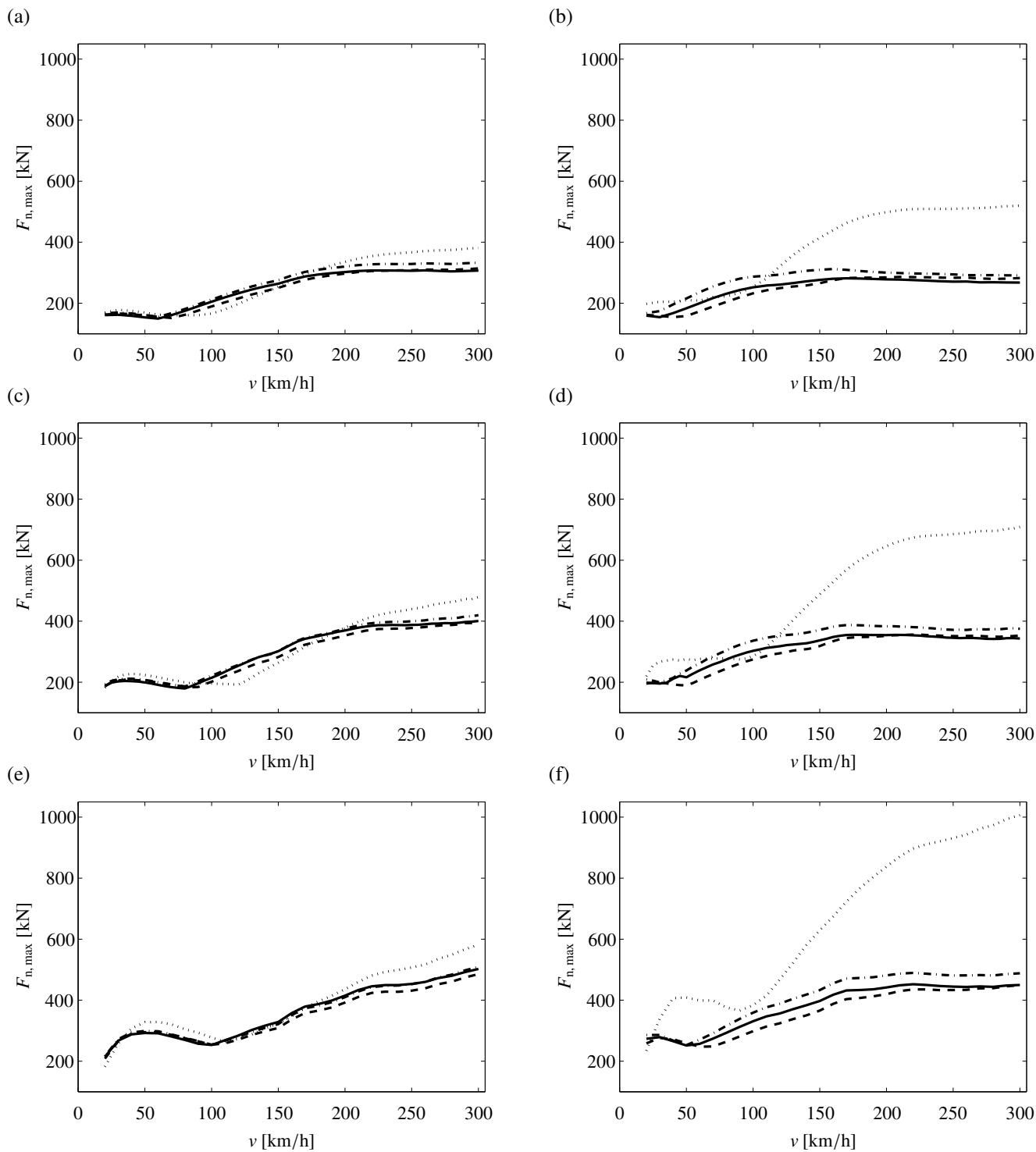


Figure 9: Maximum impact forces due to: (a) a rounded 0.5 mm deep wheel flat; (b) a newly formed 0.5 mm deep wheel flat; (c) a rounded 0.9 mm deep wheel flat; (d) a newly formed 0.9 mm deep wheel flat; (e) a rounded 1.75 mm deep wheel flat; (f) a newly formed 1.75 mm deep wheel flat; Calculations with different contact models: — 3D; --- 2D; - · - Hertz (wheel centre trajectory); · · · · Hertz (profile deviation).

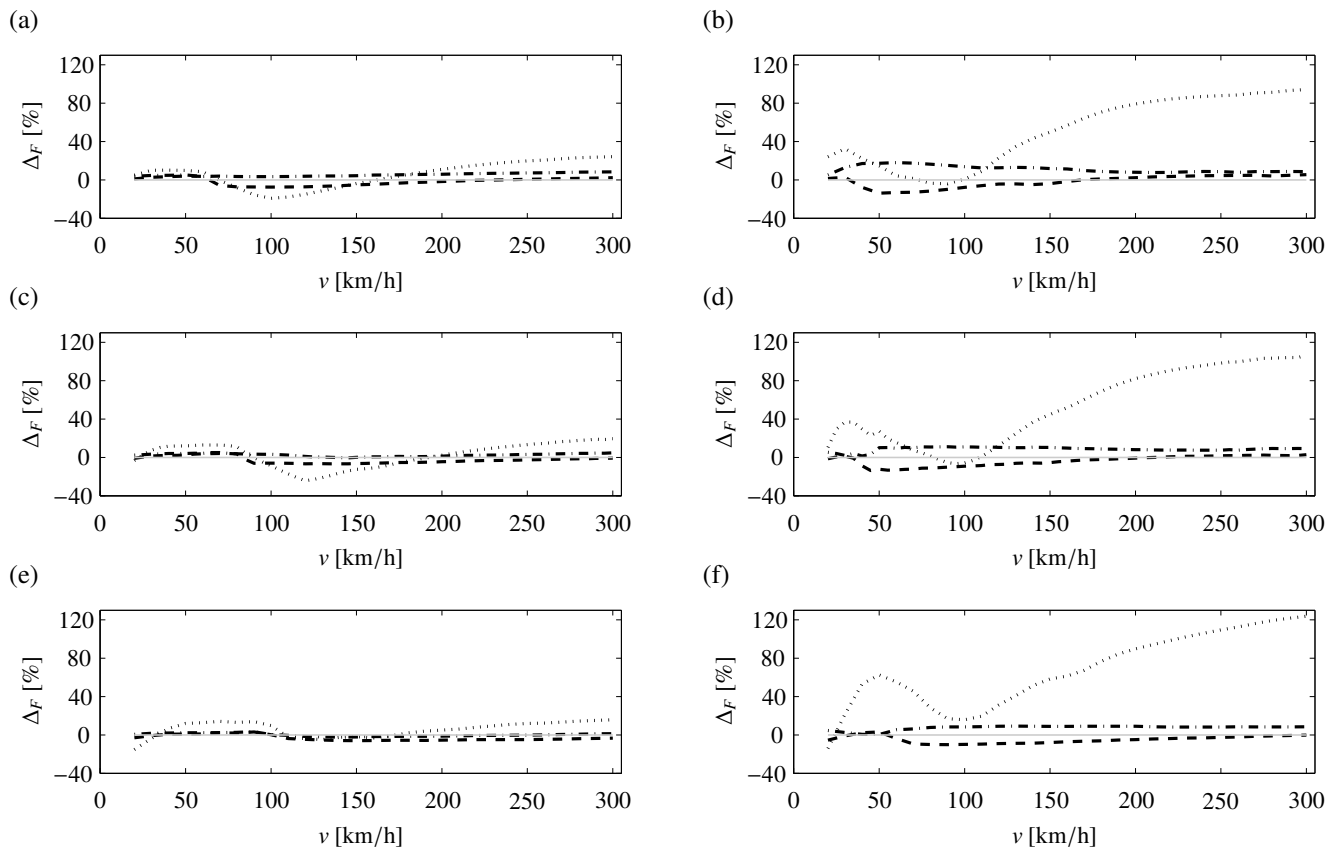


Figure 10: Relative differences  $\Delta_F = (F - F_{3D})/F_{3D}$  between the maximum impact forces from Fig. 9 obtained for the different contact models (reference 3D contact model): --- 2D; - · - Hertz (wheel centre trajectory); · · · · Hertz (profile deviation); (a) rounded 0.5 mm deep wheel flat; (b) newly formed 0.5 mm deep wheel flat; (c) rounded 0.9 mm deep wheel flat; (d) newly formed 0.9 mm deep wheel flat; (e) rounded 1.75 mm deep wheel flat; (f) newly formed 1.75 mm deep wheel flat.

Baeza et al. [11] also observed that the Hertzian model gives higher maximum impact forces than the 3D contact model in most of the cases studied, but deviations higher than 30% were reported.

Finally, the 2D contact model performs equally well as the Hertzian model based on the wheel centre trajectory, but has the tendency to underestimate the results. In the examples from Figs. 9 and 10, the deviations from the 3D contact model do not exceed 8% and 14% for the rounded and new wheel flats, respectively.

## 5. Conclusions

Four different formulations of the contact for the dynamic wheel/rail interaction caused by wheel flats have been studied and compared: a 3D non-Hertzian model, a 2D non-Hertzian model and the Hertzian model with either the wheel profile deviation or the pre-calculated wheel centre trajectory as relative displacement input.

The formulations give rather similar results with exception of the Hertzian model with the wheel profile deviation as input. In this case a substantial overestimation of the maximum impact forces can occur in comparison to the detailed 3D model. However, the magnitude of deviation from the 3D model depends

strongly on the specific case, i.e. train speed and geometry of the flat. Using instead pre-calculated wheel centre trajectories as input corrects for this shortcoming. The Hertzian contact model then gives results with approximately the same accuracy as observed in the 2D model, the former contact model having the tendency to slightly overestimate the maximum impact force and the latter to slightly underestimate.

As expected the depth of the flat is strongly determining the maximum impact force as well as the occurrence of loss of contact. In addition, large differences in maximum impact forces are observed when comparing newly formed and rounded wheel flats. From this it can be concluded that the exact geometry of the flat is an important input to the simulation. Differences in shape will lead to bigger variations in maximum impact forces than differences in the formulations of the contact (excluding the Hertzian model with the wheel profile deviation as input). Consequently, in order to reach sufficient accuracy, predictions of impact forces should rather be based on measured wheel flat geometries than simplified analytical functions.

- [1] J. Jergéus, Railway wheel flats – martensite formation, residual stresses, and crack propagation, PhD thesis, Division of Solid Mechanics, Chalmers University of Technology, Göteborg, Sweden, 1998.
- [2] D.J. Thompson, C.J.C. Jones, A review of the modelling of wheel/rail noise generation, *J. Sound Vib.* 231 (3) (2000) 519-536.
- [3] I.L. Vér, C.S. Ventres, M.M. Myles, Wheel/rail noise - Part III: Impact

- noise generation by wheel and rail discontinuities, *J. Sound Vib.* 46 (3) (1976) 395-417.
- [4] S.G. Newton, R.A. Clark, An investigation into the dynamic effects on the track of wheel flats on railway vehicles, *J. Mech. Eng. Sci.* 21 (4) (1979) 287-297.
- [5] J.M. Tunna, Wheel/rail force due to wheel irregularities, Proceedings of the Ninth International Wheelset Congress, Montreal, Canada, Paper 6-2, October 1988.
- [6] J.C.O. Nielsen, A. Igeland, Vertical dynamic interaction between train and track - influence of wheel and track imperfections, *J. Sound Vib.* 187 (5) (1995) 825-839.
- [7] R.V. Dukkipati, R. Dong, Impact loads due to wheel flats and shells, *Vehicle Syst. Dyn.* 31 (1999) 1-22.
- [8] T.X. Wu, D.J. Thompson, A hybrid model for the noise generation due to railway wheel flats, *J. Sound Vib.* 251 (1) (2002), 115-139.
- [9] M. Seco, E. Sanchez, J. Vinolas, A time domain wheelflat/track FE model, *IET Seminar Digest 2006 (11575)* (2006) 130-135.
- [10] A. Pieringer, W. Kropp, D.J. Thompson, Investigation of the dynamic contact filter effect in vertical wheel/rail interaction using a 2D and a 3D non-Hertzian contact model, *Wear* 271 (1-2) (2011) 328-338.
- [11] L. Baeza, A. Roda, J. Carballeira, E. Giner, Railway train-track dynamics for wheel flats with improved contact models, *Nonlinear Dynam.* 45 (2006) 385-397.
- [12] J.J. Zhu, A.K.W. Ahmed, S. Rakheja, An adaptive contact model for simulation of wheel-rail impact load due to a wheel flat, *Adv. Vib. Eng.* 9 (3) (2010) 215-230.
- [13] A. Pieringer, Time-domain modelling of high-frequency wheel/rail interaction, PhD thesis, Department of Civil and Environmental Engineering, Chalmers University of Technology, Göteborg, Sweden, 2011.
- [14] J.C.O. Nielsen, High-frequency vertical wheel-rail contact forces - validation of a prediction model by field testing, *Wear* 265 (2008) 1465-1471.
- [15] A. Nordborg, Wheel/rail noise generation due to nonlinear effects and parametric excitation, *J. Acoust. Soc. Am.* 111 (4) (2002) 1772-1781.
- [16] J.J. Kalker, *Three-dimensional Elastic Bodies in Rolling Contact*, Kluwer Academic Publishers, Dordrecht, 1990.
- [17] R.A.J. Ford, D.J. Thompson, Simplified contact filters in wheel/rail noise prediction, *J. Sound Vib.* 293 (2006) 807-818.
- [18] M.J.M.M. Steenbergen, The role of the contact geometry in wheel-rail impact due to wheel flats, *Vehicle Syst. Dyn.* 45 (12) (2007) 1097-1116.
- [19] K.L. Knothe, S.L. Grassie, Modelling of railway track and vehicle/track interaction at high frequencies, *Vehicle Syst. Dyn.* 22 (1993) 209-262.
- [20] A. Pieringer, W. Kropp, A time-domain model for coupled vertical and tangential wheel/rail interaction - A contribution to the modelling of curve squeal, In T. Maeda et al. (Eds.), *Noise and Vibration Mitigation for Rail Transportation Systems*, NNFEM 118, pp. 221-229, Springer, 2012.
- [21] X. Zhao, Z. Li, J. Liu, Wheel-rail impact and the dynamic forces at discrete supports of rails in the presence of singular rail surface defects, *Proc. IMechE, Part F: J. Rail and Rapid Transit* 226 (2011), 124-139.
- [22] Z. Li, X. Zhao, R. Dollevoet, M. Molodova, Differential wear and plastic deformation as causes of squat at track local stiffness change combined with other track short defects, *Vehicle Syst. Dyn.* 46, Supplement (2008), 237-246.
- [23] Z. Wen, X. Jin, W. Zhang, Contact-impact stress analysis of rail joint region using the dynamic finite element method, *Wear* 258 (2005) 1301-1309.
- [24] A. Johansson, J.C.O. Nielsen, Out-of-round railway wheels - wheel rail contact forces and track response derived from field tests and numerical simulations, *Proc. Inst. Mech. Eng. F J. Rail Rapid Transit* 217 (2003) 135-146.
- [25] J.C.O. Nielsen, J.W. Ringsberg, L. Baeza, Influence of railway wheel flat impact on crack growth in rails. Proceedings of the 8th International Heavy Haul Conference, Rio de Janeiro, Brazil, pp 789-797, June 2005.